Interfacial triferroicity in monolayer chromium dihalide

Liu Yang, Yaxin Gao, Menghao Wu, and Puru Jena

Phys. Rev. B **105**, 094101 — Published 1 March 2022

DOI: 10.1103/PhysRevB.105.094101

Interfacial Triferroicity in Chromium Dihalide Monolayer

Liu Yang[1], Yaxin Gao[1], Menghao Wu[1]*, Puru Jena[2]

[1]School of Physics, Huazhong University of Science and Technology, Wuhan, Hubei, China 430074

[2]Department of Physics, Virginia Commonwealth University, Richmond, Virginia, USA 23284

*Email: wmh1987@hust.edu.cn

Couplings between different ferroics in two-dimensional (2D) materials, with atomic thickness and van der Waals surface, has been long-sought but not yet realized. Here we show the first-principle evidence of unique triferroic couplings in recently synthesized CrI_2 monolayer. Its ferroelasticity with a low switching barrier stems from the Jahn-Teller effect. When coupled with the interaction of a substrate, a type of interfacial ferroelectricity with direction determined by the ferroelastic states can emerge which can be switched following the same low-barrier pathway of ferroelastic switching. The direction of its striped antiferromagnetism is also governed by its ferroelastic states, leading to a coupling of ferroelasticity, ferroelectricity and magnetism. Such mechanism of multiferroic couplings, denoted as interfacial Jahn-Teller triferroicity, can be applied to other 2D materials such as $CuCl_2$ and their Janus monolayers, enabling electrical manipulation of spintronics for efficient non-volatile random-access memories.

Synthesis of monolayer graphene and its spectacular properties [1] have stimulated enormous interest in the search for other two-dimensional (2D) materials with unique characteristics. For example, the existence of two-dimensional (2D) ferromagnetism in chromium trihalides was predicted [2] in 2016 and experimentally verified a year later.[3] Stimulated by the recent successful synthesis [4,5] of 2D chromium dihalide monolayer with the distorted lattice revealed by STM, in this paper we propose that it may host the coexistence of triferroics[6-8] and strong triferroic couplings that have been elusive in conventional multiferroics. It is known that ferroic materials with multiple equivalent states can be utilized as non-volatile memories, thus alleviating problems of power consumption and dissipation as well as quantum tunneling at the nanoscale in the current silicon-based memory devices. 2D materials have been explored as possible media for ferroics where their atomic thickness and clean van der Waals interface may enable high-density and high-quality integration. Aside from 2D ferromagnets, [3,9] a series of 2D ferroelectrics have been predicted [10-15] and experimentally confirmed.[16-24] However, none of the predictions of 2D ferroelasticity [25-28] has been verified due to their high switching barriers or substrate issues that lead to fracture or inequivalence between states.[29] Similarly, the predictions of 2D multiferroics [30-36] where two or more ferroics coexist are yet to be realized. In fact, multiferroic materials with two strongly coupled ferroics are rare in nature, especially for magnetic ferroelectrics where the origin of their ordering is mutually exclusive. Nevertheless, they have been long-sought because of the benefit of combining the merits of different ferroics in data reading/writing devices.[37-39] Herein, through first-principles calculations, we predict that CrI_2 monolayer is such a multiferroic material. Its low-barrier ferroelasticity originates from the Jahn-Teller (J-T) effect, which also governs the direction of its striped antiferromagnetism. Moreover, the inversion symmetry can be broken by the substrate so the two I layers, with different charges, can give rise to “interfacial” ferroelectricity fixed along the ferroelastic elongated direction. As a result, ferroelasticity, ferroelectricity and magnetism are coupled, and efficient “electrical writing + magnetic reading” can be realized.

Our theoretical calculations are based on density functional theory (DFT) implemented in the Vienna ab initio Simulation Package (VASP 5. 4) [40,41]. The exchange and correlation potentials are described within the generalized gradient approximation using the Perdew-Burke-Ernzerhof (PBE) form, together with the projector-augmented wave method.[42,43] D3 functional of Grimme [44] is used to account for the van der Waals interaction and GGA + U method with an effective U value (U_{eff}) of 7eV is used to account for strong correlation. The energy cutoff for plane waves is set to 400 eV. The convergence threshold for self-consistent-field iteration is set to 10^{-6} eV and all structures are fully optimized until the forces are smaller than 0.01 eV/ Å. $10\times10\times1$ and $4\times8\times1$ Gamma-centered k mesh [45] are adopted

to sample the first Brillouin zone of the primitive cell and $1\times\sqrt{3}\times1$ supercell, respectively. The Gaussian smearing method (with a σ value of 0.05 eV) and a Bloch-corrected tetrahedron method are used for structural relaxations and total energy calculations, respectively. The relative energies of different spin configurations and the band structure of CrI_2 monolayer is calculated by using Heyed-Scuseria-Ernzerhof (HSE) hybrid functionals [46]. It is time-consuming for optimizing the structures while the results can be approximately fitted by using PBE + U method with U_{eff} =7 eV, and the optimized lattice constants also agree well with experimental results [5]. Electrical polarizations are computed by using the Berry phase method [47], and the ferroelastic switching pathways are obtained by using solid-state nudged elastic band (SSNEB) [48] method. The vacuum layers are set to 20 Å so that the interaction between adjacent slabs can be neglected. The phonon spectra are computed by using the PHONOPY code based on the finite displacement method [49].

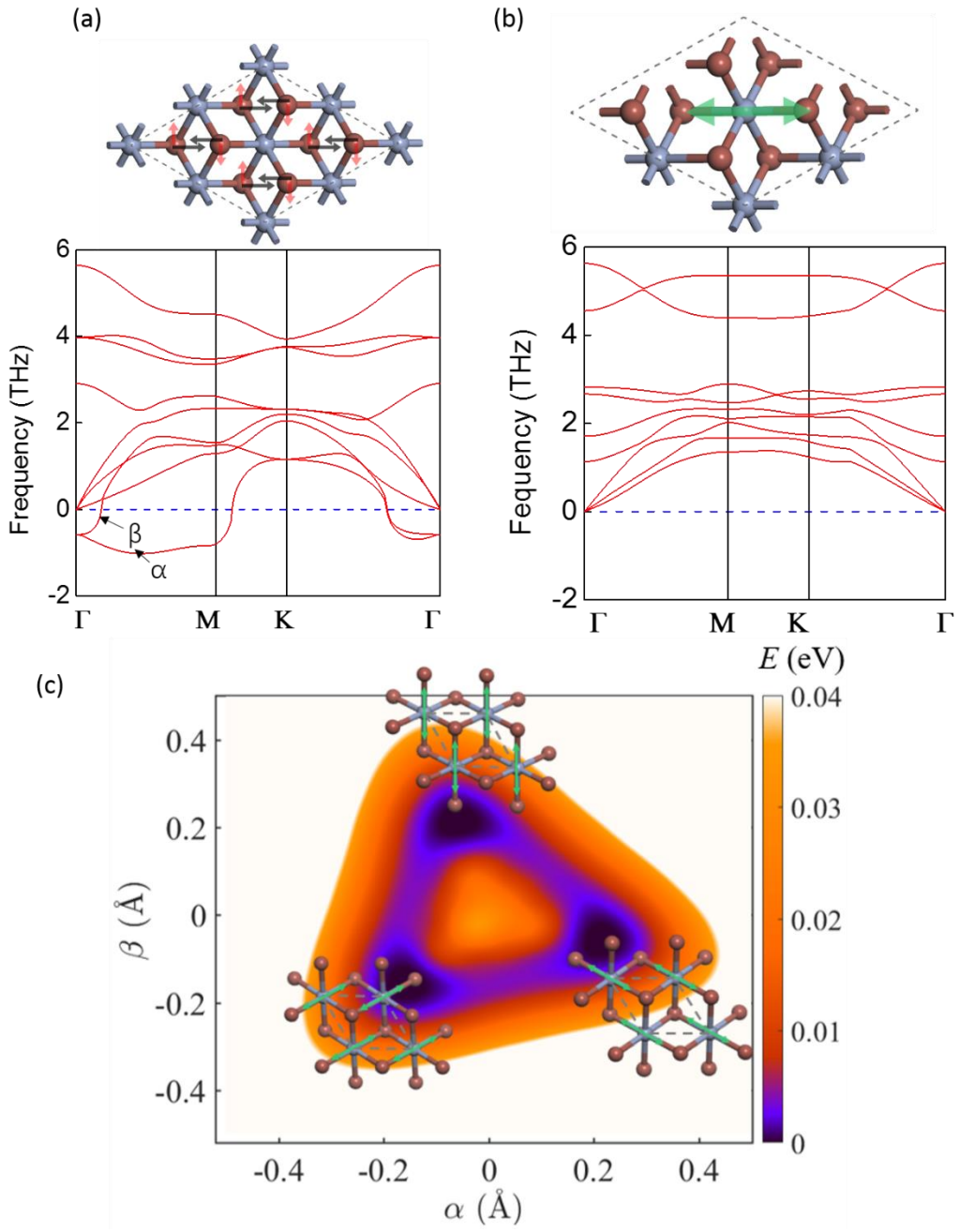

FIG. 1. Geometric structures and phonon spectra of CrI_2 monolayer (a) with symmetrical P-3M1 structures (two soft modes marked as α and β respectively correspond to the red and black arrows), and (b) the ground state with Jahn-Teller distortion (the elongated directions are marked by green arrows). (c) Energy landscape of (α, β) plane upon the combined displacements of two modes. The Cr and I atoms are denoted by dark blue and brown spheres, respectively.

It is known that many metal halide monolayers[50] form into CdI_2 structures with hexagonal close packed array in P-3M1 symmetry. When CrI_2 monolayer is made to adopt to such a symmetrical structure, as shown in Fig. 1(a), the structural instability occurs as is revealed by its phonon spectrum. Here, two imaginary soft optical modes (labelled as α and β) are closely associated with ferroelastic transition. The eigen-modes of α and β are marked by the arrow in Fig. 1(a), where the displacements of the I atoms via the combination of two modes give rise to a more stable structure. In the 2D (α, β) plane corresponding to the combination of two modes, three minima in the energy landscape corresponding to symmetry-equivalent structures can be clearly visualized. These are distorted structures elongated along either of the three directions marked by green arrows. They are all 0.08 eV per unit-cell lower in energy compared with the symmetric CdI_2 structure; its phonon spectrum without imaginary frequency in Fig. 1(b) confirms its dynamical stability. Our prediction of such a distorted 2D structure, with the optimized side length and interior angle of its unitcell (4.23 Å and 56.8 degree), agrees well with the experimental observation (4.23 Å and 55 degree).[5]

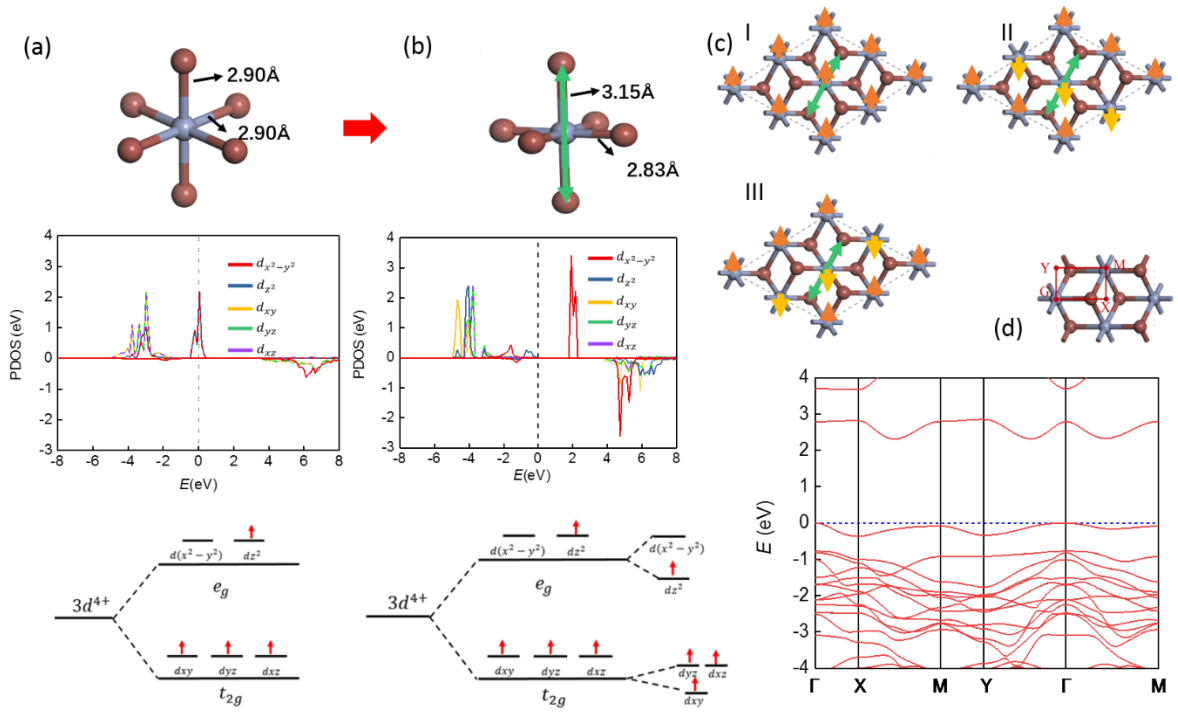

FIG. 2. The geometric structures, PDOS analysis and energy diagrams of electron occupations for Cr 3d orbitals in the Cr-I octahedral of CrI_2 (a) before and (b) after Jahn-Teller distortion. (c)Illustrations of monolayer CrI_2 with different magnetic configurations. The orange and yellow arrows respectively denote

spin-up and spin-down for Cr ions and the J-T elongated directions are marked by green arrows. (d) Bandstructure of CrI_2 monolayer in the ground state II.

For the symmetrical CdI_2 structure in Fig. 1(a), each chromium atom is bonded to six equivalent iodine atoms with the same Cr-I bond length of 2.90 Å. After distortion, each elongated octahedral is composed of two longer axial bonds of 3.15 Å and four shorter equatorial bonds of 2.83 Å, as shown in Fig. 2(b). The spontaneous distortion can be attributed to Jahn-Teller effect, according to the projected density of states (PDOS) analysis for the Cr atoms of both structures. For the ferromagnetic state, the magnetic moment of each Cr atom for both structures is 4 μ_B, indicating a high spin state (S=2, $d^{4+}(t_{2g}^3 e_g^1)$). For the structure in Fig. 1(a) with P-3M1 symmetry, as a typical octahedral crystal field splitting, the PDOS of each Cr falls into only two groups, namely triply degenerate e_g (d_{yz}, d_{xz} and d_{xy}) and doubly degenerate t_{2g} ($d_{x^2-y^2}$ and d_{z^2}) as shown in the PDOS and energy level diagram (Figure 2(a)). Nevertheless, further crystal field splitting takes place in both degenerate e_g and t_{2g} orbitals after J-T distortion as the $d_{x^2-y^2}$ orbital is un-occupied while the d_{z^2} orbital is occupied. Due to such anisotropy, the electron density along the z-axis is higher than that along other directions, giving rise to a higher electrostatic repulsion between two ligands that elongates the octahedral along the z-axis. This is consistent with the PDOS analysis.

We compare the energies of different spin configurations in Fig. 2(c) using HSE functionals, and the (II) ground state is found to be striped antiferromagnetic where the ferromagnetic spin chains are formed along the direction perpendicular to the J-T elongation, with the inter-chain coupling being antiferromagnetic, which is respectively 12.5 and 7.5 meV lower in energy compared with the (I) ferromagnetic state and (III) another stripy antiferromagnetic state. Based on the ground state (II), we calculate its bandstructure using HSE functionals in Fig. 2(d), revealing a band gap of 2.1 eV much less than the gap of 3.2 eV in previous experimental report [5]. The experimental band gap was measured at finite temperature where the system can be paramagnetic with all the spins in disorder, which is likely to be larger compared with the computed bandgap for the antiferromagnetic ground state in 0K with the spins aligned into ferromagnetic stripy channels.

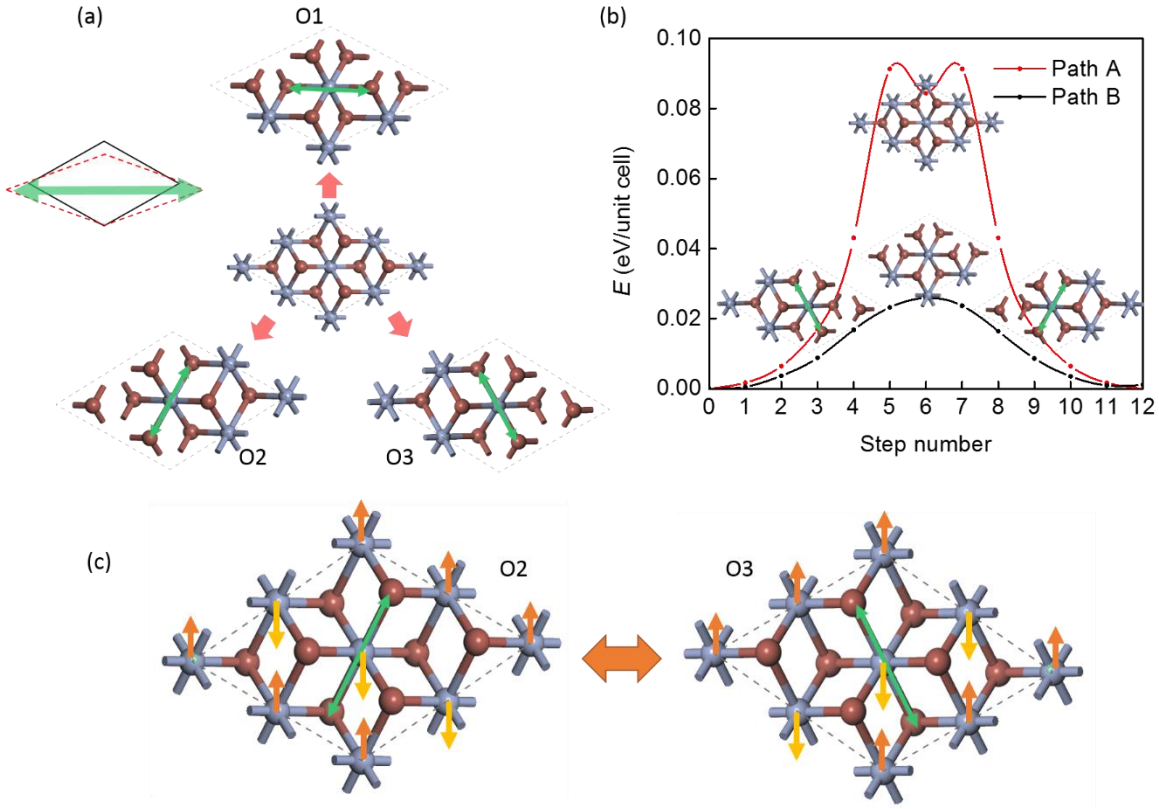

FIG. 3. (a) Three equivalent ground states and (b) ferroelastic pathway of the CrI_2 monolayer. (c) The change of spin configurations during ferroelastic switching.

The unstable undistorted-lattice can be elongated by the J-T effect along either one of the three symmetry-equivalent directions labeled by green arrows in Fig. 3(a); the three orientation states are denoted as O1, O2 and O3. Taking the O1 phase as an example, the longer diagonal length of the rhombus unitcell increases by 4.8% while the shorter diagonal length decreases by 1.3%. Now, we investigate the transformation between the three states, i. e., the ferroelastic switching by rotating the spontaneous strain by 120 degrees. With the unstable undistorted-phase is set as the intermediate state for the ferroelastic switching (path A in Fg. 3(b)), the switching barrier is found to be ~0.10 eV/unitcell. This barrier can be further reduced to ~0.02 eV/unitcell when the pathway is computed by using SSNEB method in Fig. 3(b), where the transition state is a rhombus structure with elongated shorter diagonal length. It is an order of magnitude lower compared with the predicted barrier for WTe_2 monolayer (> 0.2 eV/f.u.)[26] with similar three symmetry-equivalent states. Such a barrier indicates a much-reduced energy cost and stress required for ferroelastic switching, which facilitates practical realization and protects the material

from fracture during switching. As the J-T elongated direction rotates by 120 degrees via ferroelastic switching, the spin distribution is also altered with the 120-degree switching of antiferromagnetic stripe direction, as shown in Fig. 3(c). Therefore, the magnetism of CrI_2 is coupled with ferroelasticity.

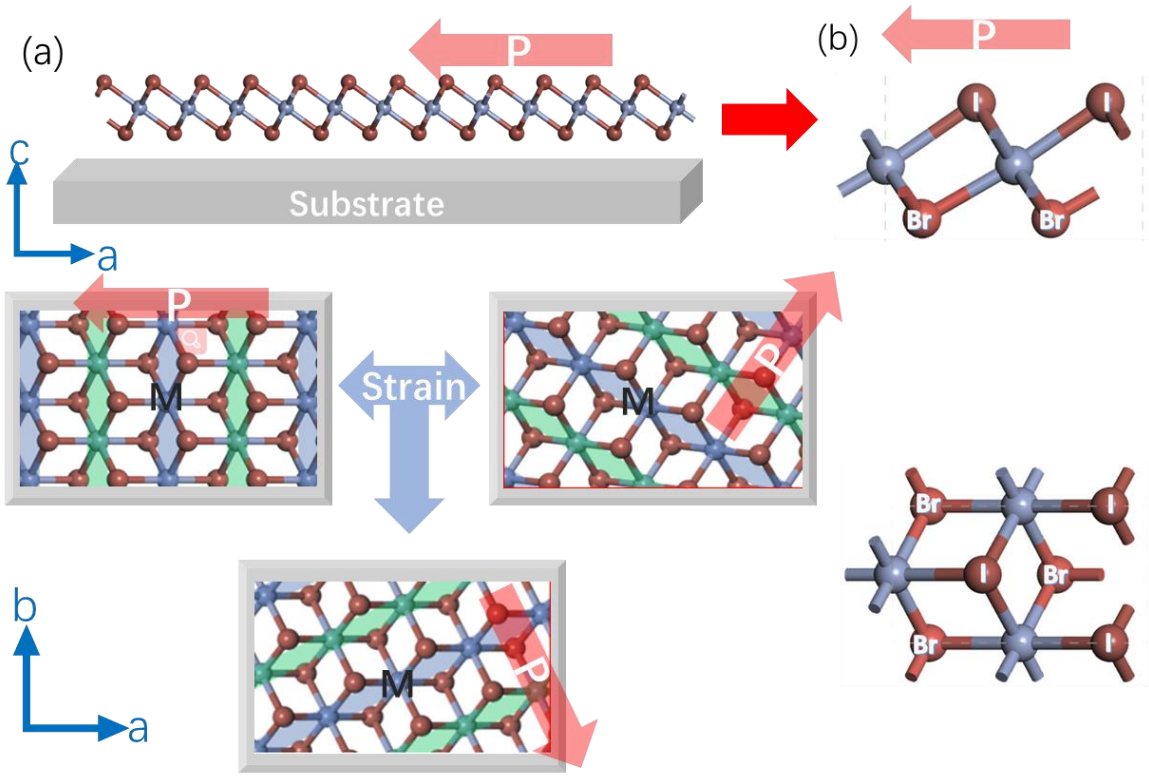

FIG. 4. (a) The in-plane polarization of CrI_2 monolayer due to the symmetrical breaking by the substrate, and its ferroelectric switching is equivalent to ferroelastic switching. (b) The CrI_2 monolayer with ferroelectricity induced by the substrate behaves akin to a Janus CrBrI monolayer.

Both the structures before and after J-T distortion in Fig. 1 are centrosymmetric and, thus, non-polar. However, the system can become polar when it interacts with the substrate as the bottom and top I atoms at the interface become inequivalent due to proximity effect (see Fig. 4(a)). Consequently, the charges on

top and bottom I atoms would be different and the induced vertical polarization cannot be switchable. In contrast, the induced in-plane polarization is fixed along the elongation direction, which can be switched by 120 degrees via either external electric field or ferroelastic switching. The substrate used in the previous experiment was graphene [5], where the symmetry of the substrate can still make the three orientation states identical and the influence of the weak interfacial van der Waals interaction on the ferroelastic switching barrier negligible. Here for the simplification of DFT simulations, we select graphene, h-BN and $ZrSe_2$ monolayer as the substrates of CrI_2 monolayer with relatively small lattice mismatch for study[51]. To our Hirshfeld charge analysis, the charges on top/bottom I atom are respectively -0.101/-0.062e, -0.101/-0.042e and -0.083/-0.039e for graphene, h-BN and $ZrSe_2$ monolayer as the substrate. Such top/bottom charge differences give rise to in-plane switchable polarizations of CrI_2 monolayer, which are respectively 1.43 and 0.58 pC/m on substrate BN and $ZrSe_2$ (screened on semi-metallic graphene). We also note that the inequivalence between the two I atom layers due to the substrate makes the monolayer behave like a 2D Janus structure (e.g., CrBrI), noting that 2D Janus structure like MoSSe has been experimentally synthesized with different charges on S and Se layers [52]. For the Janus CrBrI shown in Fig. 4(b), the charge on Br and I are respectively -0.145e and -0.085e according to the Hirshfeld analysis, and the in-plane polarization is estimated to be ~2pC/m. Such a polarization can be switched by 120 degrees by applying an external electric field following the same pathway as ferroelastic switching. Here, the orientation of spin stripes will also rotate by 120 degrees. Therefore, ferroelectricity, ferroelasticity and magnetism are all coupled, and such triferroic couplings can be used to control the magnetism via ferroelectric switching that is equivalent to ferroelastic switching. This can make efficient "electric writing + magnetic reading" possible. Hence, electrically-controlled giant anisotropic magnetoresistance for non-volatile memories can be realized in such 2D triferroics, which is highly desirable but still challenging in the current developing field of antiferromagnetic spintronics.[53] As mentioned above, the stripy antiferromagnetic ground state is only 12.5 meV lower in energy compared with the ferromagnetic state in Fig. 2, which is far below the ~k_BT at room temperature, so the system will be paramagnetic and cannot be utilized for antiferromagnetic spintronic applications at ambient conditions; meanwhile the distorted ground state is 0.08 eV higher in energy compared with the symmetrical state (corresponding to the paraelastic and paraelectric state) in Fig. 1, making the ferroelasticity and ferroelectricity robust against thermal fluctuation at room temperature, which is also confirmed by our MD simulation at 300K[51]. Similar coexistence and coupling between ferroelasticity and ferroelectricity may exist in a series of 2D materials with similar lattices and substrates, like $CrCl_2$/$CrBr_2$, $CuCl_2$, ZrI_2, $MoTe_2$/WTe_2, etc., as well as their corresponding Janus monolayers.

In summary, using calculations based on density functional theory, we reveal a unique 2D interfacial triferroicity and triferroic couplings in previously synthesized CrI_2 monolayer, which is hitherto unreported and to be experimentally confirmed. The future experimental realization of its ferroelasticity stemming from Jahn-Teller distortion can be facilitated not only by its low switching barrier, but also by the symmetry of graphene substrate, making the three orientation states still identical. Combination of Jahn-Teller distortion and interfacial interaction with the substrate further leads to ferroelectricity. Strong coupling among its striped antiferromagnetism, ferroelasticity and ferroelectricity can enable electrical manipulation of spintronics, making efficient non-volatile random-access memories possible. Such multiferroic couplings via combined distortion and interfacial effect can be applied to a series of 2D materials with similar lattices and their corresponding Janus monolayers, thus stimulating experimental efforts.

Acknowledgement

MW is supported by the National Natural Science Foundation of China (Nos. 22073034). P.J. acknowledges partial supported by the U.S. Department of Energy, Office of Basic Energy Sciences, Division of Materials Sciences and Engineering under Award DE-FG02-96ER45579.

L. Y and Y. G. contributed equally to this work.

References

[1] K. S. Novoselov, A. K. Geim, S. V. Morozov, D. Jiang, Y. Zhang, S. V. Dubonos, I. V. Grigorieva, and A. A. Firsov, Science **306**, 666 (2004).
[2] J. Liu, Q. Sun, Y. Kawazoe, and P. Jena, Phys. Chem. Chem. Phys. **18**, 8777 (2016).
[3] B. Huang, G. Clark, E. Navarro-Moratalla, D.R. Klein, R. Cheng, K.L. Seyler, D. Zhong, E. Schmidgall, M.A. McGuire, D.H. Cobden *et al.*, Nature **546**, 270 (2017).
[4] X. Cai, Z. Xu, S.-H. Ji, N. Li, and X. Chen, Chin. Phys. B **30**, 028102 (2021).
[5] L. Peng, J. Zhao, M. Cai, G.-Y. Hua, Z.-Y. Liu, H.-N. Xia, Y. Yuan, W.-H. Zhang, G. Xu, L.-X. Zhao *et al.*, Phys. Rev. Res. **2**, 023264 (2020).
[6] L. Yang, M. Wu, and K. Yao, Nanotechnology **29**, 215703 (2018).
[7] Y. Gao, M. Wu, and X. C. Zeng, Nanoscale Horiz. **4**, 1106 (2019).
[8] Y. Gao, M. Wu, and P. Jena, Nat. Commun. **12**, 1331 (2021).
[9] C. Gong, L. Li, Z. Li, H. Ji, A. Stern, Y. Xia, T. Cao, W. Bao, C. Wang, Y. Wang *et al.*, Nature **546**, 265 (2017).
[10] M. Wu and X. C. Zeng, Nano Lett. **16**, 3236 (2016).
[11] R. Fei, W. Kang, and L. Yang, Phys. Rev. Lett. **117**, 097601 (2016).

[12] S. N. Shirodkar and U. V. Waghmare, Phys. Rev. Lett. **112**, 157601 (2014).
[13] W. Ding, J. Zhu, Z. Wang, Y. Gao, D. Xiao, Y. Gu, Z. Zhang, and W. Zhu, Nat. Commun. **8**, 14956 (2017).
[14] L. Li and M. Wu, ACS nano **11**, 6382 (2017).
[15] M. Wu and X. C. Zeng, Nano Lett. **17**, 6309 (2017).
[16] K. Chang, J. Liu, H. Lin, N. Wang, K. Zhao, A. Zhang, F. Jin, Y. Zhong, X. Hu, W. Duan *et al.*, Science **353**, 274 (2016).
[17] N. Higashitarumizu, H. Kawamoto, C.-J. Lee, B.-H. Lin, F.-H. Chu, I. Yonemori, T. Nishimura, K. Wakabayashi, W.-H. Chang, K. Nagashio, Nat. Commun. **11**, 2428 (2020).
[18] P. Sutter, H. P. Komsa, H. Lu, A. Gruverman, and E. Sutter, Nano Today **37**, 101082 (2021).
[19] C. Zheng, L. Yu, L. Zhu, J.L. Collins, D. Kim, Y. Lou, C. Xu, M. Li, Z. Wei, Y. Zhang *et al.*, Sci. Adv. **4** (2018).
[20] F. Liu, L. You, K.L. Seyler, X. Li, P. Yu, J. Lin, X. Wang, J. Zhou, H. Wang, H. He *et al.*, Nat Commun **7**, 12357 (2016).
[21] A. Belianinov, Q. He, A. Dziaugys, P. Maksymovych, E. Eliseev, A. Borisevich, A. Morozovska, J. Banys, Y. Vysochanskii, S.V. Kalinin, Nano Lett. **15**, 3808 (2015).
[22] H. Hu, Y. Sun, M. Chai, D. Xie, J. Ma, and H. Zhu, Appl. Phys. Lett. **114**, 252903 (2019).
[23] P. Sharma, F.-X. Xiang, D.-F. Shao, D. Zhang, E. Y. Tsymbal, A. R. Hamilton, and J. Seidel, Sci. Adv. **5**, eaax5080 (2019).
[24] Z. Fei, W. Zhao, T. A. Palomaki, B. Sun, M. K. Miller, Z. Zhao, J. Yan, X. Xu, and D. H. Cobden, Nature **560**, 336 (2018).
[25] M. Wu, H. Fu, L. Zhou, K. Yao, and X. C. Zeng, Nano Lett. **15**, 3557 (2015).
[26] W. Li and J. Li, Nat Commun **7**, 10843 (2016).
[27] L. Kou, Y. Ma, C. Tang, Z. Sun, A. Du, and C. Chen, Nano Lett **16**, 7910 (2016).
[28] X. Li, L. Li, and M. Wu, Mater. Today Phys. **15**, 100229 (2020).
[29] Z. Tu and M. Wu, Sci. Bull. **65**, 147 (2020).
[30] J.-J. Zhang, L. Lin, Y. Zhang, M. Wu, B. I. Yakobson, and S. Dong, J. Am. Chem. Soc. **140**, 9768 (2018).
[31] W. Luo, K. Xu, and H. Xiang, Phys.Rev.B **96**, 235415 (2017).
[32] T. Zhong, X. Li, M. Wu, and J.-M. Liu, Natl. Sci. Rev. **7**, 373 (2019).
[33] Z. Tu and M. Wu, Adv. Electron. Mater. **5**, 1800960 (2019).
[34] Q. Yang, W. Xiong, L. Zhu, G. Gao, and M. Wu, J. Am. Chem. Soc. **139**, 11506 (2017).
[35] C. Huang, Y. Du, H. Wu, H. Xiang, K. Deng, and E. Kan, Phys. Rev. Lett. **120**, 147601 (2018).
[36] Q. Yang, T. Zhong, Z. Tu, L. Zhu, M. Wu, and X. C. Zeng, Adv Sci (Weinh) **6**, 1801572 (2019).
[37] S. Dong, H. Xiang, and E. Dagotto, Natl. Sci. Rev. **6**, 629 (2019).
[38] C.-W. Nan and J.-M. Liu, Natl. Sci. Rev. **6**, 620 (2019).
[39] C. Lu, M. Wu, L. Lin, and J.-M. Liu, Natl. Sci. Rev. **6**, 653 (2019).
[40] G. Kresse and J. J. P. r. B. Furthmüller, Phys.Rev.B **54**, 11169 (1996).
[41] G. Kresse and J. J. C. m. s. Furthmüller, Comput. Mater. Sci. **6**, 15 (1996).
[42] J. P. Perdew, K. Burke, and M. J. P. r. l. Ernzerhof, Phys. Rev. Lett. **77**, 3865 (1996).
[43] P. E. J. P. r. B. Blöchl, Phys.Rev.B **50**, 17953 (1994).
[44] S. Grimme, J. Antony, S. Ehrlich, and H. J. T. J. o. c. p. Krieg, J. Chem. Phys. **132**, 154104 (2010).
[45] M. Methfessel and A. J. P. R. B. Paxton, Phys.Rev.B **40**, 3616 (1989).
[46] J. Heyd, G. E. Scuseria, and M. Ernzerhof, J. Chem.Phys. **118**, 8207 (2003).
[47] R. King-Smith and D. J. P. R. B. Vanderbilt, Phys.Rev.B **47**, 1651 (1993).
[48] G. Henkelman, B. P. Uberuaga, and H. J. T. J. o. c. p. Jónsson, J. Chem. Phys. **113**, 9901 (2000).
[49] A. Togo and I. J. S. M. Tanaka, Scr. Mater. **108**, 1 (2015).
[50] M. Wu, 2D Mater. **4**, 021014 (2017).

[51] See Supplemental Material at[URL will be inserted by publisher] for some heterostructure designs and the MD simulations of CrI_2 monolayer.
[52] A.-Y. Lu, H. Zhu, J. Xiao, C.-P. Chuu, Y. Han, M.-H. Chiu, C.-C. Cheng, C.-W. Yang, K.-H. Wei, Y. Yang *et al.*, Nat. Nanotechnol. **12**, 744 (2017).
[53] P. Wadley, B. Howells, J. Železný, C. Andrews, V. Hills, R.P. Campion, V. Novák, K. Olejník, F. Maccherozzi, S.S. Dhesi *et al.*, Science **351**, 587 (2016).